



## Article

# Anisotropic Differences in the Thermal Conductivity of Rocks: A Summary from Core Measurement Data in East China

Yibo Wang <sup>1,2</sup>, Zhuting Wang <sup>3,\*</sup>, Lin Shi <sup>4</sup>, Yuwei Rong <sup>4</sup>, Jie Hu <sup>5</sup> , Guangzheng Jiang <sup>1,2</sup> , Yaqi Wang <sup>1,2,6</sup> and Shengbiao Hu <sup>1,2,6</sup>

- <sup>1</sup> State Key Laboratory of Lithospheric Evolution, Institute of Geology and Geophysics, Chinese Academy of Sciences, Beijing 100029, China; ybwang@mail.iggcas.ac.cn (Y.W.); guangzheng@mail.iggcas.ac.cn (G.J.); wangyaqi@mail.iggcas.ac.cn (Y.W.); sbhu@mail.iggcas.ac.cn (S.H.)
- <sup>2</sup> Innovation Academy for Earth Science, Chinese Academy of Sciences, Beijing 100864, China
- <sup>3</sup> School of Mines, China University of Mining and Technology, Xuzhou 221116, China
- <sup>4</sup> The Seventh Institute of Geology and Mineral Exploration of Shandong Province, Linyi 276006, China; shilin112010@outlook.com (L.S.); rongyuwei111@outlook.com (Y.R.)
- <sup>5</sup> State Key Laboratory of Oil and Gas Reservoir Geology and Exploitation, Chengdu University of Technology, Chengdu 610225, China; hujiel61@mails.ucas.ac.cn
- <sup>6</sup> College of Earth and Planetary Sciences, University of Chinese Academy of Sciences, Beijing 100049, China
- \* Correspondence: wangzhuting123@cumt.edu.cn; Tel.: +86-010-8299-8533

**Abstract:** The study of thermal conductivity anisotropy is of great importance for more accurate heat flow calculations, geodynamic studies, development and utilization of hot dry rock, and simulation of heat transfer in geological reservoirs of nuclear waste, and so on. To study the thermal conductivity anisotropy of rocks, 1158 cores from 60 boreholes in East China were tested for thermal conductivity, including thermal conductivity values parallel to ( $\lambda_{\parallel}$ ) and perpendicular to ( $\lambda_{\perp}$ ) structural planes of basalt, mudstones, gneisses, sandstones, carbonates, evaporites, and metamorphic rocks. The thermal conductivity anisotropy is not obvious for sand, clay, and evaporate, and the average anisotropic factors of  $1.19 \pm 0.22$ ,  $1.18 \pm 0.17$ , and  $1.18 \pm 0.17$  for tuff/breccia, granitoid and contact metamorphic rocks, respectively, indicate that these three rocks have strong anisotropy characteristics. Finally, the effect of thermal conductivity anisotropy on heat flow is studied and discussed in detail, showing that the results of thermal conductivity tests have a significant effect on the calculation of heat flow and thermal structure, and the data show that a deviation of about 10% in thermal conductivity causes a deviation of about 11% in heat flow, which may lead to a misperception of deep thermal structure studies. The regular and anisotropic characteristics of thermal conductivity of various rocks in Eastern China obtained in this paper can provide parameter support for projects such as heat flow calculations, thermal structure studies, and geothermal resource development and utilization.

**Keywords:** thermal conductivity; anisotropy; anisotropic factor; East China; cores



**Citation:** Wang, Y.; Wang, Z.; Shi, L.; Rong, Y.; Hu, J.; Jiang, G.; Wang, Y.; Hu, S. Anisotropic Differences in the Thermal Conductivity of Rocks: A Summary from Core Measurement Data in East China. *Minerals* **2021**, *11*, 1135. <https://doi.org/10.3390/min11101135>

Academic Editor: Pieter Bertier

Received: 10 September 2021

Accepted: 12 October 2021

Published: 15 October 2021

**Publisher's Note:** MDPI stays neutral with regard to jurisdictional claims in published maps and institutional affiliations.



**Copyright:** © 2021 by the authors. Licensee MDPI, Basel, Switzerland. This article is an open access article distributed under the terms and conditions of the Creative Commons Attribution (CC BY) license (<https://creativecommons.org/licenses/by/4.0/>).

## 1. Introduction

Most objects in nature are anisotropic, characterized by having different properties in different directions in space. The anisotropy of rocks has been one of the key points and difficulties in the field of engineering. Thermal conductivity, as an important thermophysical property of rocks, is closely related to the texture, structure, mineral composition, and external environment of rocks, and shows obvious anisotropy in space. In many previous studies, the thermal conductivity of rocks was often considered to be isotropic, such as in the simulation of seepage and heat transfer in rocks around nuclear waste disposal [1], numerical simulation of geothermal development of oil wells [2,3], and geothermal development of high-temperature rocks [4,5]. However, the setting of isotropic rock thermal conductivity does not fully reflect the actual heat transfer processes in the rock mass and differs significantly from the actual situation.

The thermal conductivity anisotropy of rock is universal, mainly manifested in the following aspects: (1) the thermal conductivity values of different minerals vary widely, and the difference in mineral composition and content can lead to different bulk thermal conductivity of the rock [6]; (2) some crystalline rocks are affected by external environmental changes during the rock formation process, resulting in a certain orientation of the spatial arrangement of minerals; (3) the laminated structure of most sedimentary rocks is highly anisotropic and, in addition, different cementation types can affect the overall thermal conductivity values. [7]; (4) regional metamorphic deformation, or tectonic rocks in the formation process, where the minerals will undergo obvious stretching, directional arrangement, etc., forming anisotropic structural surfaces. Extensive studies have shown the importance of considering the anisotropy of thermal conductivity for heat flow calculations, geodynamic studies, development of hot dry rock, and heat transfer simulations for geological repositories of nuclear waste.

In this study, we measured 1158 core samples from 60 boreholes in East China (Figure 1), tested the thermal conductivity values parallel ( $\lambda_{\parallel}$ ) and perpendicular ( $\lambda_{\perp}$ ) to the structural plane, respectively, and calculated the anisotropy coefficients. East China is usually referred to as the region where the third terrace of China's landforms is located, which is bounded by the NE–SW-trending Daxinganling-Taihang Mountains-Xuefeng Mountains in the west and the western Pacific Ocean in the east, and consists of several first-order tectonic units such as the Northeast, North China, South China and Central Orogenic Belt unit (Figure 1). Based on the data, we studied the trends of thermal conductivity and anisotropic factor, and their correlations according to different lithologies, and discussed in detail the implications of thermal conductivity testing on heat flow calculations and lithospheric thermal structure studies.

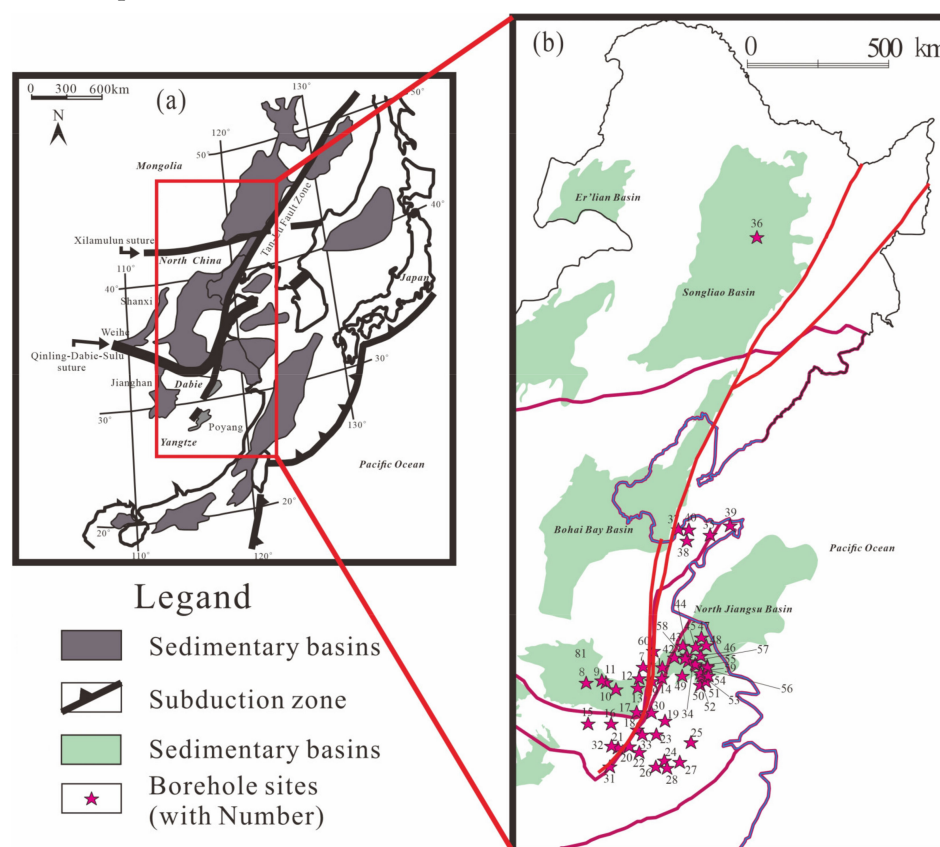


**Figure 1.** (a) Schematic geological map in East Asia (modified after [8]); (b) distribution of borehole locations for this study; (b) is an enlargement of the red rectangle in (a).

## 2. Measurement of Thermal Conductivity

### 2.1. Sample Preparation

The 1158 core samples in this experiment were taken from 60 boreholes (Figure 1, Table 1) within the depth range of 0–4130 m in East China, including 64 basalt and andesite samples, 49 tuff and breccia samples, 267 granitoid samples, 145 coal and mudstone samples, 123 sandstone and conglomerate samples, 94 carbonate samples, 148 contact metamorphic rock samples, 150 regional metamorphic rock samples, 45 sand samples, 64 clay samples, and 9 evaporite samples.

**Table 1.** Comprehensive information on the boreholes where the cores were located.

Serial Number	Borehole	Longitude	Latitude	Rang of Depth for Heat Flow Calculation	Number	Lithology
		E	N	Z (m)	1158	
1	Dang-1	116°30'58"	34°31'44"	600–1100	29	mudstone, evaporite
2	Bo-1	115°46'44"	33°48'26"	790–1500	13	mudstone, sandstone
3	Fu-1	115°21'23"	33°14'19"	690–1500	14	mudstone, sandstone
4	Bo-2	115°45'42"	33°53'10"	1090–2300	14	sandstone
5	Sui-1	116°34'55"	33°37'9"	300–620	16	mudstone, sandstone, carbonate
6	Huai-1	116°50'51"	33°58'60"	260–1590	25	mudstone, sandstone, carbonate, granitoid
7	Wu-1	117°50'13"	33°9'40"	580–1300	23	mudstone, sandstone, carbonate, coal
8	Fu-2	115°35'9"	32°52'13"	390–1300	18	mudstone, sandstone
9	Ying-1	116°20'36"	32°48'52"	460–1300	46	mudstone, sandstone, carbonate, coal
10	Shou-1	116°41'36"	32°32'51"	580–1920	20	sandstone, gneiss
11	Ban-1	116°11'34"	32°53'26"	690–1000	15	carbonate, sandstone
12	Feng-1	117°37'44"	32°48'33"	180–420	17	leptynite, amphibolite, gneiss
13	Ding-1	117°31'42"	32°30'29"	70–420	28	mudstone, evaporite
14	Lai-1	118°29'35"	32°42'49"	60–270	17	basalt, granitoid, mudstone
15	Jin-1	115°29'22"	31°32'45"	270–750	19	granitoid
16	Huo-1	116°21'23"	31°27'22"	30–250	23	gneiss, breccia
17	He-1	117°22'1"	31°43'54"	570–1510	28	sandstone, mudstone
18	Lu-1	117°18'24"	31°10'12"	80–220	30	hornstone
119	Huai-2	116°55'44"	30°39'24"	340–950	26	hornstone
20	Tong-1	117°16'28"	30°26'9"	180–530	31	carbonate
21	Tong-2	117°59'33"	30°55'48"	150–270	19	silica rock
22	Huang-1	118°9'34"	30°3'32"	130–980	42	sandstone, mudstone, dolerite
23	Ning-1	119°14'8"	30°31'17"	190–570	21	granitoid
24	Qi-1	117°48'46"	29°53'51"	140–590	24	carbonate, mudstone, slate
25	Huang-2	118°43'1"	29°56'50"	360–500	13	granitoid
26	Xiu-1	118°13'18"	29°48'40"	10–250	22	sandstone, mudstone
27	Ming-1	118°5'48"	32°39'40"	100–800	16	phyllite, schist
28	Ban-2	117°55'8"	31°38'59"	80–500	13	carbonate
29	Huang-3	118°43'1"	29°56'50"	40–810	18	phyllite
30	Su-1	116°7'12"	30°5'23"	1240–1570	4	mudstone, sandstone
31	Xi-1	116°16'22"	30°44'44"	200–460	5	diorite, schist
32	LZSD	117°28'5"	30°58'59"	0–3000	147	granitoid, tuff, andesite
33	Huang-4	118°9'26"	30°11'48"	210–1170	15	granitoid
34	SR-1	119°51'51"	32°57'18"	850–4130	27	carbonate, sandstone, mudstone
35	Ru-1	121°13'59"	37°4'47"	110–550	16	leptynite
36	SKSD	125°38'47"	46°14'27"	1100–2780	24	sandstone, mudstone
37	Lai-2	119°59'57"	37°25'19"	230–3980	39	granitoid, gneiss
38	Ping-1	120°16'15"	37°0'43"	50–850	17	granitoid
39	Wen-1	122°6'5"	37°16'4"	100–2000	40	granitoid
40	Zhao-1	120°25'5"	37°21'42"	100–3000	40	granitoid

Table 1. Cont.

Serial Number	Borehole	Longitude	Latitude	Rang of Depth for Heat Flow Calculation	Number	Lithology
		E	N		1158	
41	SB-1	118°34'6"	33°3'45"	40–200	3	sand, clay, sandstone, mudstone
42	SB-2	119°5'9"	33°19'8"	40–200	4	sand, clay, sandstone, mudstone
43	SB-3	119°28'35"	33°39'37"	40–200	5	sand, clay, sandstone, mudstone
44	SB-4	119°34'13"	33°19'36"	40–200	6	sand, clay, sandstone, mudstone
45	SB-5	119°57'31"	33°33'21"	40–200	8	sand, clay, sandstone, mudstone
46	SB-6	120°6'5"	33°14'48"	40–200	10	sand, clay, sandstone, mudstone
47	SB-7	120°14'4"	33°49'57"	40–200	5	sand, clay, sandstone, mudstone
48	SB-8	120°22'17"	33°33'17"	40–200	5	sand, clay, sandstone, mudstone
49	SB-9	119°16'34"	32°41'43"	40–200	6	sand, clay, sandstone, mudstone
50	SB-10	119°54'30"	32°18'44"	40–200	5	sand, clay, sandstone, mudstone
51	SB-11	120°8'38"	32°23'57"	40–200	3	sand, clay, sandstone, mudstone
52	SB-12	120°1'1"	32°35'35"	40–200	5	sand, clay, sandstone, mudstone
53	SB-13	119°59'15"	32°41'33"	40–200	5	sand, clay, sandstone, mudstone
54	SB-14	120°16'3"	32°34'13"	40–200	5	sand, clay, sandstone, mudstone
55	SB-15	120°17'8"	32°53'42"	40–200	10	sand, clay, sandstone, mudstone
56	SB-16	119°50'13"	33°0'19"	1480–1500	2	sand, clay, sandstone, mudstone
57	SB-17	119°35'11"	33°7'52"	980–1000	2	sand, clay, sandstone, mudstone
58	SB-18	119°29'16"	33°14'27"	780–800	2	sand, clay, sandstone, mudstone
59	SBTZK3	120°17'13"	32°50'41"	50–730	14	sand, clay, sandstone, mudstone
60	Jin-2	118°18'44"	33°37'47"	150–2200	39	gneiss, schist, marble

All the samples were obtained by core drilling with full-size boreholes (cores over ten centimeters in length). Through actual measurement, the anisotropy angle of all sedimentary rock samples selected in this study was within 10°. In addition, it was assumed that the anisotropic angle of both magmatic and metamorphic rocks was zero in this study.

The sample pretreatment included four main steps: (a) cutting and flattening of the cylinder top and bottom surface (Figure 2a)—the surface of the sample is cut flat (no other mechanical treatment, such as polishing, etc.) to ensure that the spatial deviations of the test surface are within 0.5 mm; (b) wiping—using an abrasive cloth and towel to wipe the test surface clean; (c) painting (Figure 2b)—every sample is painted by a black enamel along every scanning line chosen (approximately 20 mm in width and 25–40 µm in thickness); and (d) drying (Figure 2c)—the thermal conductivity measurements must be started after full drying of samples only (usually one day).

## 2.2. Measurement Method

The thermal conductivity of rocks ( $\lambda$ ) is a measure of the rock thermal conductivity, defined as the amount of heat per unit time that passes through a unit area per unit length of an object, along the direction of heat transfer, when the temperature of the object decreases by 1 °C, in W/m/K. The most commonly used test method in geothermics is the optical scanning method [9], which has been successfully tested for the thermal conductivity of cores from the ultra-deep drilling in the Kola Peninsula, Russia, and the first China Continental Scientific Drilling [10,11]. The thermal conductivity scanner (TCS, TCS Version 2) manufactured by Lippmann and Rauen GbR, Schaufling, Germany, was used for this research, and its measurement range was 0.2–25.0 W/m/K with an accuracy of  $\pm 3\%$ . During the test, the instrument scans the samples through a concentrated, moving, and continuous heat source and calculates the thermal conductivity from the difference in the temperature values received by the infrared temperature sensor before and after the heat source scan and by comparison with standard samples with known thermal conductivity (Figure 2d,e). It should be noted that the standard samples selected differed



for different samples, and the standard samples that are closer to the test sample have less error in the test.

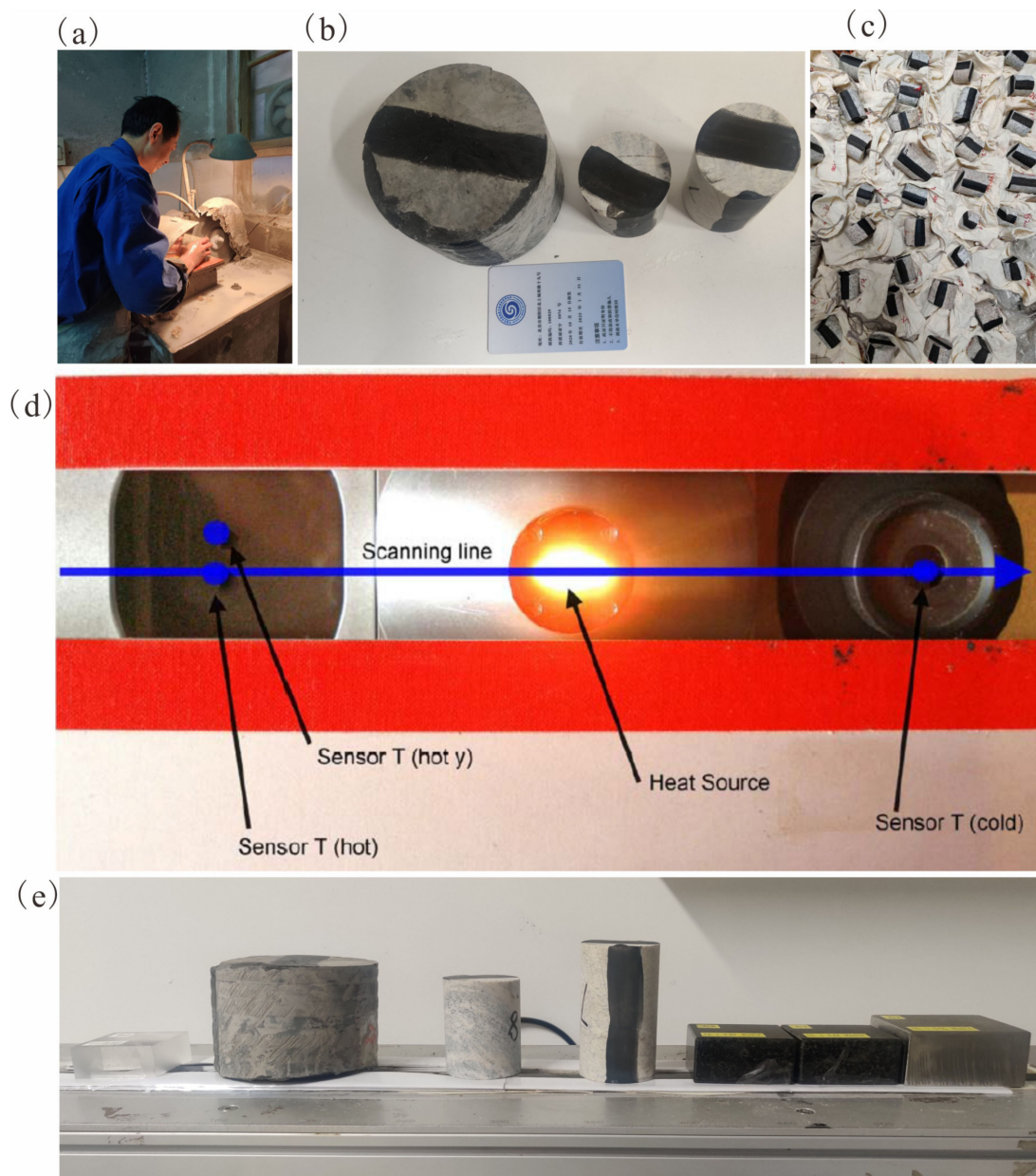


**Figure 2.** Preparation and TCS measurement of core samples. (a) Flattening of the cylinder top and bottom surface; (b) painting of the test surface; (c) drying; (d) thermal conductivity scanner with 2-channel “hot” sensor and 1-channel “cold” sensor; (e) the flat platform of TCS, where standards and samples were placed.

### 3. Anisotropic Thermal Conductivity

#### 3.1. Anisotropic Model of Thermal Conductivity

It is generally accepted that rock anisotropy affects its thermal conductivity [7,12–14]. The results of previous studies on the thermal conductivity and thermal conductivity anisotropy of rocks are shown in Table 2. The anisotropic factor tends to decrease gradually as time advances and the number of measured samples increases, such as in sandstones and limestone [7,13,15,16], which may imply that more samples need to be tested and statistically analyzed.

**Table 2.** Anisotropy of thermal conductivity of rocks in previous studies.

Rock Type	$\lambda_{\parallel}$ (W/m/K)	Number of Measured Samples for $\lambda_{\parallel}$	$\lambda_{\perp}$ (W/m/K)	Number of Measured Samples for $\lambda_{\perp}$	Anisotropic Factor (A)	Reference
Gneiss	7.19	1	5.08	1	1.42	Birch and Clark, 1940 [13]
Limestone	7.9	1	5.9	1	1.34	Birch and Clark, 1940 [13]
Marble	6.9	1	6.7	1	1.03	Birch and Clark, 1940 [13]
Gneiss, schist	8.55	17	6.95	15	1.23	Birch, 1950 [17]
Gneiss	8.9	8	6.34	22	1.4	Clark and Niblett, 1956 [18]
Schist	7.5	7	5.74	8	1.31	Clark and Niblett, 1956 [18]
Gneiss, mica	9.32	6	6.27	12	1.49	Clark and Niblett, 1966 [19]
Sandstone	7.74	17	7.14	17	1.08	Hurtig, 1965 [16]
Gneiss, schist	10.74	7	7.23	8	1.49	Clark, 1961 [20]
Granite gneiss	8.87	13	6.85	9	1.29	Clark, 1961 [20]
Gneiss	8.33	9	6.24	9	1.33	Clark, 1961 [20]
Quartzite, gneiss	11.8	4	7	4	1.69	Sass and Le Marne, 1963 [21]
Schist, gneiss	8.61	34	6.62	35	1.3	Diment and Werre, 1964 [22]
Gneiss, schist	7.01	10	5.51	10	1.27	Diment and others, 1965 [23]
Dolomite	9.5	61	9.35	58	1.02	Meincke et al., 1967 [15]
Sandstone	5.46	19	4.59	28	1.19	Meincke et al., 1967 [15]
Slate, schist	6.03	2	3.62	2	1.67	Meincke et al., 1967 [15]
Anhydrite	8.71	12	8.54	13	1.02	Robertson, 1988 [24]
Phyllite	11.83	9	7.89	7	1.5	Robertson, 1988 [24]
Quartzitic sandstone	12.6	1	12.2	1	1.03	Robertson, 1988 [24]
Gneiss, amphibolite	3.1	81	2.56	81	1.21	Pribnow and Sass, 1995 [25]
Clay	0.85	6	0.72	6	1.18	Midttomme et al., 1998 [26]
Mudstone	1.17	9	0.81	9	1.45	Midttomme et al., 1998 [26]
Limestone	3.18	7	3.19	7	1	Davis et al., 2007 [7]
Sandstone	4.06	10	3.95	10	1.03	Davis et al., 2007 [7]
Shale	2.73	6	2.56	6	1.08	Davis et al., 2007 [7]
Argillite	4.8	15	4.21	15	1.23	Davis et al., 2007 [7]
Quartzite	6.41	6	7.06	6	0.91	Davis et al., 2007 [7]
Granodiorite	2.59	11	2.59	11	1	Davis et al., 2007 [7]
Monzonite	2.78	17	2.76	17	1.01	Davis et al., 2007 [7]

Through measurement and modeling of the thermal conductivity of sedimentary rock samples, Midttomme and Roaldset [27] found that the thermal conductivity measurements parallel to the mineral grains can be up to twice as high as the perpendicular measurements. However, after conducting thermal conductivity tests on rock samples, it was concluded by Davis et al. [7] that the anisotropic factor was close to 1.0 in some rock types (limestone, monzonite, and granodiorite), or even less than 1.0 (quartzite). Wu et al. [12] tested the thermal conductivity of different samples parallel to and perpendicular to the structural plane in the Songliao basin and proposed segmentation functions to fit the variation of anisotropic factors of different rock types. In recent years, numerical simulations have

been gradually introduced into experimental analysis for the study of anisotropy and heterogeneity of rock thermal conductivity [28].

Thermal conductivity can be deemed as a second-order tensor and it follows the rotational transformation criterion. Therefore, the thermal conductivity values after anisotropic correction can be obtained through the following equation [29]:

$$\lambda'_{ab} = \lambda_{ij} \times \alpha_{ai} \times \alpha_{bj} \quad (1)$$

where  $\lambda'_{ab}$  is the thermal conductivity after rotation transformation;  $\lambda_{ij}$  is the measured thermal conductivity;  $\alpha_{ai}$  and  $\alpha_{bj}$  are the elements of the direction cosine.

Besides, if the parallel and perpendicular thermal conductivity is known, the thermal conductivity of a rock sample in a specific anisotropic angle ( $\theta$ ) can be calculated by the following equation [30]:

$$\lambda(\theta) = \lambda_{\perp} \cos^2 \theta + \lambda_{\parallel} \sin^2 \theta \quad (2)$$

where  $\lambda(\theta)$  denotes the thermal conductivity at a certain anisotropic angle ( $\theta$ );  $\lambda_{\parallel}$  and  $\lambda_{\perp}$  represent the thermal conductivity parallel to and perpendicular to the structural plane, respectively.

The anisotropic factor of thermal conductivity,  $A$ , of a given rock sample can be defined as the ratio of the thermal conductivity parallel to the structural plane to that perpendicular, that is:

$$A = \lambda_{\parallel} / \lambda_{\perp} \quad (3)$$

### 3.2. Anisotropic Model in This Research

The anisotropy of the rock thermal conductivity can be characterized by calculating the anisotropic factor for different rock samples. If the anisotropic factor is approximately 1.0, the thermal conductivity of the rock is considered isotropic. If the factor is greater than 1.10 or less than 0.95 (the standard deviation should be within 0.20), the thermal conductivity of the rock can be deemed as anisotropic, which means that the reliability of the thermal conductivity test needs to be evaluated when performing heat flow calculations, thermal history recovery, geothermal field studies, and so on.

Three models were adopted to explore the relationship between the two: (a) mean model; (b) unary linear regression (without intercept) model; (c) unary linear regression model.

In the mean value model, we calculated the parallel and vertical thermal conductivities in turn, and based on the anisotropy coefficient  $A$ , we calculated the arithmetic mean and the harmonic mean of the anisotropy coefficients for different rock types. As for the other two unary linear regression models, we used regression analysis to obtain regression parameters (coefficient, SEM) for both models, and show regression statistics, including multiple  $R$ ,  $R$  square,  $p$ -value, and significance  $F$ .

## 4. Results

### 4.1. Anisotropy of Thermal Conductivity of Different Rock Types

In the statistical analysis of the thermal conductivity data, we plotted the variation of thermal conductivity for different lithologies using  $\lambda_{\perp}$  and  $\lambda_{\parallel}$  as the horizontal and vertical axes, respectively (Figure 3). Figure 3a–d shows the anisotropic results of the thermal conductivity of magmatic and volcanic rocks, sedimentary rocks, metamorphic rocks, and unconsolidated rocks. It shows that most of the samples, except for unconsolidated sand (sand and clay), show a clear anisotropic trend, i.e.,  $\lambda_{\parallel} > \lambda_{\perp}$ . In other words, previous thermal conductivity test work performed on the perpendicular structural plane of the cores probably underestimated the true thermal conductivity values of the rocks, and the difference between the  $\lambda_{\perp}$  and  $\lambda_{\parallel}$  values cannot be ignored.

Statistical analysis shows that the anisotropic factor of different boreholes with similar lithologies does not deviate much because the selected core samples have been strictly screened. Therefore, our statistics of the anisotropic factor of the thermal conductivity

A for samples with different lithologies are significant. We calculated A for all cores using Equation (3) and analyzed the anisotropy of different rocks using the mean value model (Table 3), where a greater or lesser A value represents a more anisotropic rock. The results show that the anisotropic factor A fluctuates between 0.39 and 2.08 for all rocks, with an average value of  $1.14 \pm 0.18$ . For granitoid and tuff/breccia, the value of  $\lambda_{\parallel}$  increases significantly with the increase of  $\lambda_{\perp}$ , and the corresponding A value also increases gradually, showing strong anisotropy characteristics, with an average A of  $1.18 \pm 0.17$  and  $1.18 \pm 0.22$ , respectively; compared with the first two types, the A values of basalt and andesite are slightly smaller, with an average value of  $1.15 \pm 0.16$ ; the anisotropic factor of sedimentary rocks are generally small, with A values of  $1.16 \pm 0.15$  for carbonate rocks,  $1.10 \pm 0.14$  and  $1.14 \pm 0.16$  for sandstone/conglomerate and mudstone/coal, respectively; contact metamorphic rocks (leptynite, quartzite, marble, etc.) have significant anisotropy, comparable to granitoid ( $\alpha = 1.18 \pm 0.17$ ), with greater increases in  $\lambda_{\parallel}$  values as the  $\lambda_{\perp}$  value increases, while regional metamorphic rocks (slate, micrite, gneiss, etc.) have an A value of only  $1.11 \pm 0.14$ ; unconsolidated rocks like clay and sand, with an average A value of about 1.0, have insignificant anisotropy; evaporite have extremely high thermal conductivity values of over 5.0 W/m/K. The average A value of evaporite is  $1.12 \pm 0.20$ , but overall, no significant synergistic variation is shown between  $\lambda_{\perp}$  and  $\lambda_{\parallel}$ .

In the other two unary linear regression models, we obtained the thermal conductivity anisotropy relations for different lithologies in both  $\lambda_{\parallel}$  and  $\lambda_{\perp}$  using regression analysis with and without intercept, respectively (Table 3). According to the regression results in Table 3, there are some differences in the anisotropic relationships of thermal conductivity or anisotropy factors for different models. Compared with the simple mean model, these two linear regression models, especially the unary linear regression model, can reflect the relationship between  $\lambda_{\parallel}$  and  $\lambda_{\perp}$  more precisely, and the regression analysis often comes with detailed regression parameters, including the reliability of the results, the goodness of fit, and so on. However, conversely, the mean model more simply reflects the ratio relationship between  $\lambda_{\parallel}$ ,  $\lambda_{\perp}$ , and the anisotropic factor, and is more commonly used in practical anisotropy studies.

#### 4.2. Thermal Conductivity and Its Anisotropic Factor vs. Depth

The vertical variation of thermal conductivity has been explored by many researchers, especially in some scientific drilling on a global scale [11,31–33]. The detailed conductivity tests performed on cores from 60 boreholes in this study provides good conditions to investigate the correlation between thermal conductivity and its anisotropic factor with depth.

To reduce the interference of other factors, we selected 27 wells with relatively stable lithology and certain sampling spacing, analyzed and explored the relationship between thermal conductivity and sampling depth parallel to the structural plane  $\lambda_{\parallel}$ , and plotted the variation of thermal conductivity with depth for different boreholes (Figure 4). The trends of thermal conductivity with depth are classified in Figure 4, and the positive, no (basically stable), negative, and no (irregular fluctuations) correlations of thermal conductivity vs. depth are demonstrated in Figure 4 with increasing depth, respectively. The thermal conductivity of sandstone is generally positively correlated with depth (B9 and B41, Figure 4a); basalt and conglomerate also exhibit an increase in thermal conductivity with depth; the thermal conductivity of unconsolidated samples and evaporite is generally uncorrelated with depth at shallow depth (B46 and B59, Figure 4d); most common rocks, such as granite, mudstone and carbonates, may show a variety of thermal conductivity values that increase, decrease, remain essentially constant, or fluctuate irregularly with depth (Figure 4).



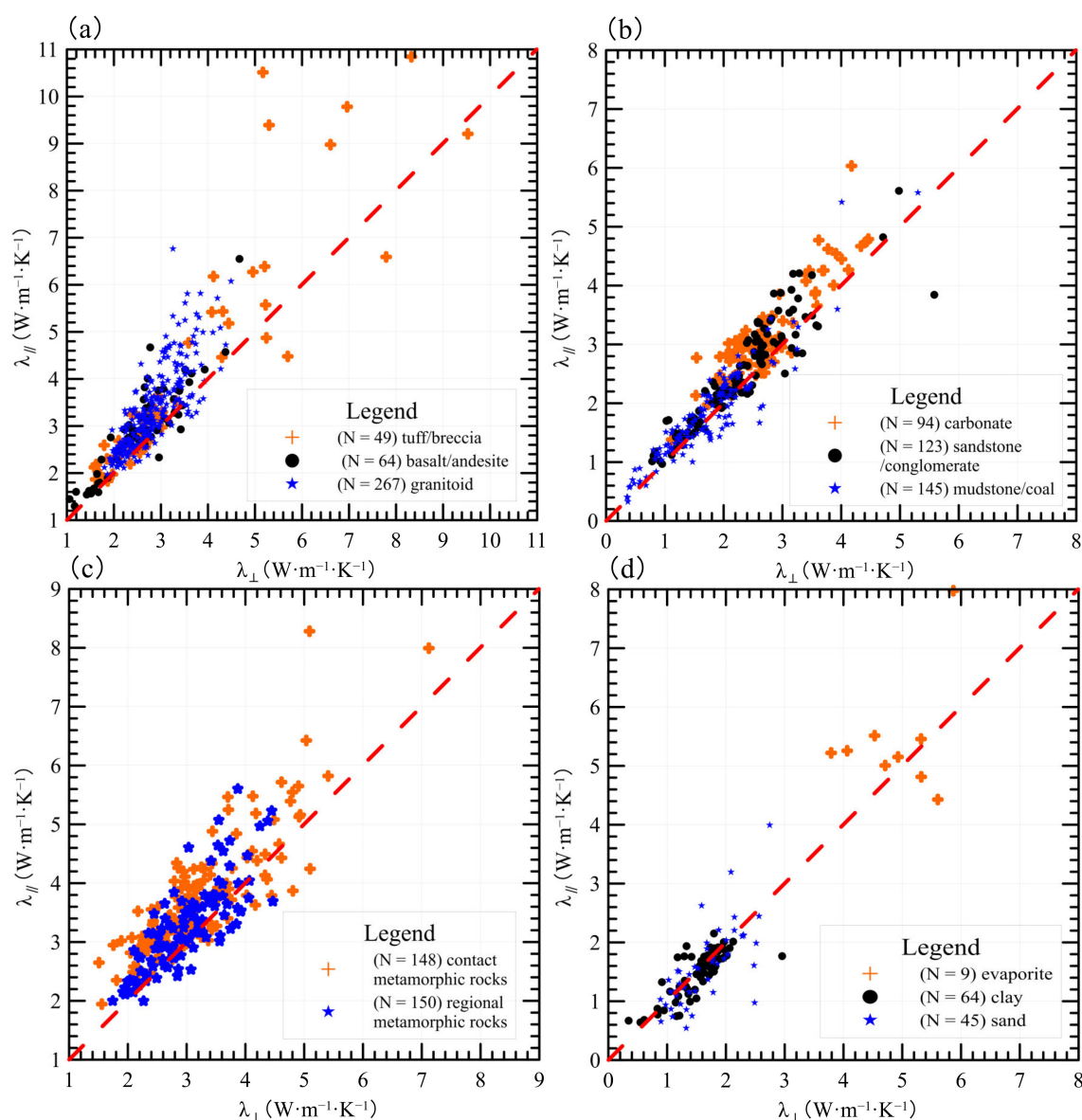


**Figure 3.** Statistical analysis of anisotropy of thermal conductivity of different rock types: (a) tuff/breccia, basalt/andesite, and granitoid; (b) carbonate, sandstone/conglomerate, and mudstone/coal; (c) contact metamorphic rocks, regional metamorphic rocks; (d) evaporite, clay, and sand.

As mentioned above, we obtained the variation of the anisotropic factor with depth for each representative borehole, as shown in Figure 5. The following conclusions can be drawn from the figure: (1) only a small portion of the rocks exhibit an increasing  $A$  value with increasing depth, and this increasing trend is not significant (Figure 5a); (2) the anisotropic factor of most of the cores show a tendency to decrease gradually with increasing depth, that is, the measured thermal conductivity anisotropy tend to gradually decrease with increasing depth; (3) the  $A$  value fluctuations of most rocks decrease significantly with increasing depth (B4, Figure 5a; B10, Figure 5b; B40, Figure 5c; B13, Figure 5d), and the improvement rate of the standard deviation of the anisotropic factor can reach more than 77% from shallow to deep (B33, Figure 5a).

**Table 3.** Statistics of anisotropic models of thermal conductivity.

Lithology	Number		Mean Model		Unary Linear Regression (Without Intercept) Model							The Unary Linear Regression Model						
	1158	Average	Harmonic Mean	SD	Coefficients 1	SEM	<i>p</i> -Value	Significance F	Multiple R	R Square	SEM	Coefficients 2	Intercept	SEM	<i>p</i> -Value/Significance F	Multiple R	R Square	SEM
Basalt, andesite	64	1.15	1.13	0.16	1.14	0.02	$2.92 \times 10^{-55}$	$1.28 \times 10^{-54}$	0.99	0.98	0.44	1.08	0.15	0.07	$1.14 \times 10^{-21}$	0.88	0.77	0.44
Tuff, breccia	49	1.19	1.15	0.22	1.19	0.04	$6.64 \times 10^{-33}$	$1.88 \times 10^{-32}$	0.97	0.95	1.10	1.17	0.06	0.08	$3.55 \times 10^{-18}$	0.90	0.80	1.12
Granitoid	267	1.18	1.16	0.17	1.19	0.01	$5.71 \times 10^{-222}$	$2.35 \times 10^{-221}$	0.99	0.98	0.52	1.26	0.20	0.06	$2.78 \times 10^{-62}$	0.81	0.65	0.51
Mudstone (coal)	145	1.14	1.12	0.16	1.04	0.01	$3.62 \times 10^{-118}$	$1.43 \times 10^{-117}$	0.99	0.98	0.31	0.96	0.16	0.03	$7.07 \times 10^{-62}$	0.92	0.86	0.30
Sandstone/conglomerate	123	1.10	1.08	0.14	1.07	0.01	$3.98 \times 10^{-107}$	$1.79 \times 10^{-106}$	0.99	0.98	0.36	0.96	0.30	0.04	$1.05 \times 10^{-49}$	0.92	0.84	0.35
Carbonate	94	1.16	1.14	0.15	1.14	0.01	$7.62 \times 10^{-89}$	$4.05 \times 10^{-88}$	0.99	0.99	0.37	1.00	0.38	0.06	$1.30 \times 10^{-31}$	0.88	0.78	0.36
Contact metamorphic rocks	148	1.18	1.16	0.17	1.14	0.01	$4.90 \times 10^{-125}$	$2.08 \times 10^{-124}$	0.99	0.98	0.56	0.91	0.81	0.05	$1.57 \times 10^{-39}$	0.83	0.70	0.52
Regional metamorphic rocks	150	1.11	1.09	0.14	1.09	0.01	$4.61 \times 10^{-131}$	$2.09 \times 10^{-130}$	0.99	0.98	0.46	0.89	0.61	0.06	$1.18 \times 10^{-31}$	0.78	0.60	0.44
Sand	45	0.95	0.88	0.26	0.96	0.04	$2.98 \times 10^{-26}$	$6.92 \times 10^{-26}$	0.96	0.92	0.48	0.95	0.02	0.14	$4.57 \times 10^{-8}$	0.71	0.50	0.49
Clay	64	0.99	0.96	0.21	0.97	0.02	$6.56 \times 10^{-55}$	$2.84 \times 10^{-54}$	0.99	0.98	0.22	0.83	0.22	0.07	$2.07 \times 10^{-17}$	0.83	0.69	0.22
Evaporite	9	1.12	1.08	0.20	1.10	0.07	$2.81 \times 10^{-7}$	$1.07 \times 10^{-6}$	0.98	0.97	1.04	0.50	2.99	0.51	$3.67 \times 10^{-1}$	0.34	0.12	1.02

Note: SD: standard deviation; SEM: standard error of the mean.

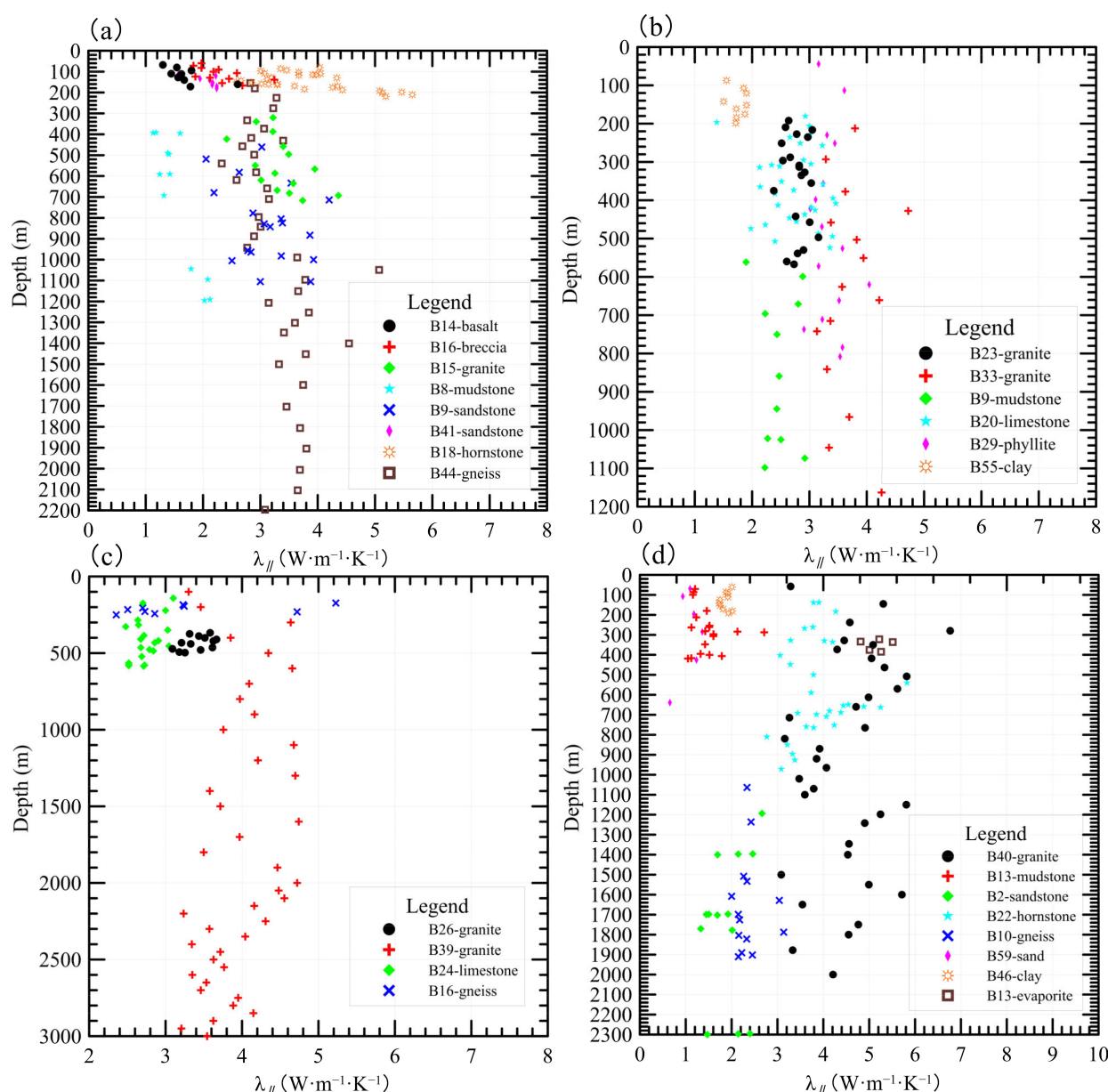


**Figure 4.** Relationship between thermal conductivity and depth: (a) examples of increasing thermal conductivity of rocks with depth; (b) examples of rocks with little variation in thermal conductivity with depth; (c) examples of decreasing thermal conductivity of rocks with depth; (d) examples of irregular fluctuations in the thermal conductivity of rocks with depth (B14: number 14 borehole in Table 1).

In the discussion of factors affecting thermal conductivity, some researchers are accustomed to choosing the relationship between thermal conductivity and depth for their analysis. The thermal conductivity of sandstone is generally positively correlated with depth (B9 and B41 in Figure 4a), but there will still be sandstones that exhibit irregular variation with depth (B2 in Figure 4d); as another example, the variation of thermal conductivity with depth for granites can show four cases including increasing (B15), constant (B33), decreasing (B39) and irregular (B40). For unconsolidated rocks, such as sand and mud, the variation of thermal conductivity vs. depth is irregular, partly because such rocks are very shallowly exposed and lithologically highly variable, and partly because the porosity of such rocks has no significant control on thermal conductivity due to similar compaction. Depth affects the distribution of thermal conductivity, but essentially, this

effect is jointly influenced by changes in other conditions, so when discussing changes in thermal conductivity, the changes in various factors, such as porosity, should be considered as comprehensively as possible, rather than just depth as the main influencing parameter.

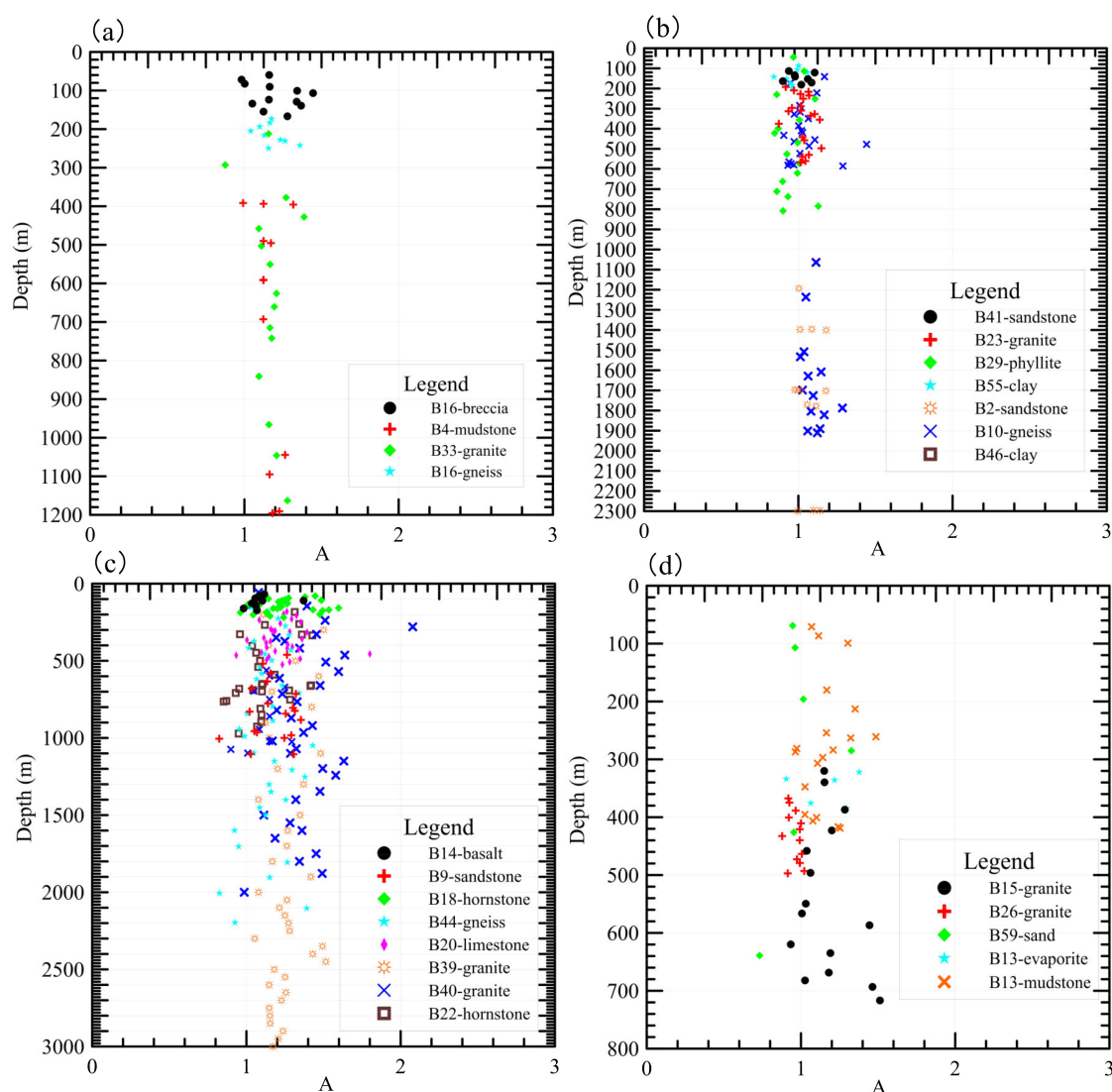


**Figure 5.** Relationship between the anisotropic factor of thermal conductivity and depth: (a) examples of increasing anisotropic factor of thermal conductivity with depth; (b) examples of little variation in the anisotropic factor of thermal conductivity with depth; (c) examples of decreasing anisotropic factor of thermal conductivity with depth; (d) examples of irregular fluctuations in the anisotropic factor of thermal conductivity with depth.

## 5. Influence of Different Thermal Conductivity Measurement Surfaces on the Study of Heat Flow and Thermal Structure

Heat flow is the most fundamental element of theoretical geothermics, characterizing the amount of heat transferred from the Earth's interior to the surface and then emitted to the atmosphere per unit time and unit area. The lithospheric thermal structure refers to the proportion of heat flow between the crust and mantle of a region and its grouping relationship, as well as the temperature distribution inside the lithosphere and the thickness of the thermal lithosphere, which is the basic representation of the present-day thermal state of the region. The study of heat flow and thermal structure provides important constraints for understanding and appreciating plate tectonics, lithospheric geophysical properties, tectono-thermal evolution, and other geodynamic processes.

Since heat flow cannot be measured directly, the current method is based on Fourier's law, which states that heat flow is numerically equal to the product of the temperature gradient at steady-state conditions and the thermal conductivity of the core corresponding to the stable section of the gradient. In the calculation of heat flow values, the following three principles are followed: (1) discard the sections with shallow water levels; (2) for the rocks in each adjacent section, the essence of the solid earth range is the "series of thermal resistance", so the inverse distance-weighted average should be used to determine the thermal conductivity of the study section. Boreholes B7 and B17 are located in the southern North China Basin of the eastern North China Craton. Combining the obtained steady-state temperature logs and lithology histograms, we obtained the heat flow values of boreholes B7 and B17 according to the method from Wang et al. [34] and Wang et al. [35], which are very close to the background heat flow in the southern North China Basin (56 mW/m<sup>2</sup>).

To explore the influence of thermal conductivity measurements on heat flow calculations and thermal structure studies, we assumed that the average heat flow values of boreholes B7 and B17 represent the regional background values, and chose three thermal conductivity models to constrain the heat flow values: model 1, in which the thermal conductivity  $\lambda_{\parallel}$  is corrected for temperature, pressure, and saturation [35]; model 2, in which the thermal conductivity  $\lambda_{\perp}$  is corrected for temperature, pressure, and saturation; and model 3, using the uncorrected thermal conductivity  $\lambda_{\perp}$ . The thermal conductivity and heat flow calculated by the three models are shown in Table 4. The heat flow values calculated by model 2 are significantly smaller than that of model 1, with an average deviation of about 11%, indicating that the thermal conductivity anisotropy has a significant effect on the calculation of heat flow values; while the deviation of model 3 is about 4% compared with model 2, which implies that even for sandstones with large porosity, the temperature, pressure and saturation correction or no correction of the thermal conductivity do not have a great effect on the heat flow values. Therefore, it is appropriate and necessary to pay more attention to the anisotropy of the thermal conductivity of cores in conducting heat flow calculations.

**Table 4.** Heat flow constrained by different thermal conductivity calculation models.

Borehole Number		B7	B17
Depth (m)		660–1300	550–1328
Temperature gradient (°C/km)		30.2	28.5
SD (°C/km)		0.9	0.3
Number (thermal conductivity)		23	19
Heat flow calculation 1	$\lambda_{\parallel}$ after correction (W/m/K)	1.9	2
	SD (W/m/K)	0.3	0.2
	Heat flow 1 (mW/m <sup>2</sup> )	56.9	56
	SD (mW/m <sup>2</sup> )	9.2	6.3
Heat flow calculation 2	$\lambda_{\perp}$ after correction (W/m/K)	1.7	1.8
	SD (W/m/K)	0.4	0.2
	Heat flow 2 (mW/m <sup>2</sup> )	49.9	51
	SD (mW/m <sup>2</sup> )	11.7	6.4
Heat flow calculation 3	$\lambda_{\perp}$ (W/m/K)	1.5	1.8
	SD (W/m/K)	0.4	0.2
	Heat flow 3 (mW/m <sup>2</sup> )	46.3	50.1
	SD (mW/m <sup>2</sup> )	11.3	6.5

Note: SD: standard deviation.



**Table 5.** Crustal layered structure and characteristics of thermal structure for different models.

Parameter		Model 1	Model 2	Model 3
Surface heat flow ( $\text{mW}/\text{m}^2$ )		56.5	50.5	48.2
Heat flow at the bottom boundary of the sedimentary strata ( $\text{mW}/\text{m}^2$ )		50.2	44.2	41.9
Heat flow at the bottom boundary of the upper crust ( $\text{mW}/\text{m}^2$ )		39.5	33.5	31.2
Heat flow at the bottom boundary of the middle crust ( $\text{mW}/\text{m}^2$ )		30.9	24.9	22.6
Mantle heat flow $q_m$ ( $\text{mW}/\text{m}^2$ )		27.9	21.9	19.6
Crust heat flow $q_c$ ( $\text{mW}/\text{m}^2$ )		28.6	28.6	28.6
Crust–mantle heat flow ratio		1.0	1.3	1.5
Thermal thickness	Maximum (km)	131.5	184.3	218.9
	Minimum (km)	117.1	166.3	198.6
	Average (km)	124.3	175.3	208.8
The temperature at the bottom boundary of the lithosphere	Maximum ( $^{\circ}\text{C}$ )	1352.6	1373.7	1387.6
	Minimum ( $^{\circ}\text{C}$ )	1258.6	1283.2	1299.3
	Average ( $^{\circ}\text{C}$ )	1305.6	1328.4	1343.4

Based on the heat flow calculation, we acquired the lithospheric thermal structure characteristics for each of the three models, as shown in Table 5. Model 1 represents the more reliable background thermal information of the region; the crust heat flow and mantle heat flow are very close, and the ratio between crust and mantle heat flow  $q_c/q_m$  is about 1.0, indicating that the region is a “warm mantle and warm crust” type thermal structure feature. The  $q_c/q_m$  calculated in models 2 and 3 are 1.3 and 1.5, respectively, characterizing that the main heat flow contribution of the region is from the crust, which is contrary to the regional thermal background [36,37]. In the study of deep thermal structure, a difference of about 10% for the surface heat flow can cause errors in the thermal structure properties, which in turn may lead to a misunderstanding of the deep dynamics background.

The thermal lithosphere thicknesses were calculated according to the method in Wang and Furlong et al. [36,38] and are shown in Table 5. Combining the aforementioned data, we plotted the thermal thickness of different models (Figure 6). The study showed that the thermal thickness obtained from model 1 is more reliable, fluctuating from 117 to 131 km, with an average thickness of 124 km, which probably represents the lithosphere thickness of the partially modified craton [36]. The average thickness of the thermal lithosphere obtained by model 3 is 209 km, which deviates from the values from [36,37]. The comparison revealed that the temperature of the lithospheric bottom boundary is generally lower in regions with thin thermal lithosphere thickness; for example, the average temperature of the lithosphere bottom boundary of model 1 is 1306  $^{\circ}\text{C}$ ; on the contrary, the average temperature of the lithosphere bottom boundary is higher, calculated by model 3 as 1343  $^{\circ}\text{C}$ .

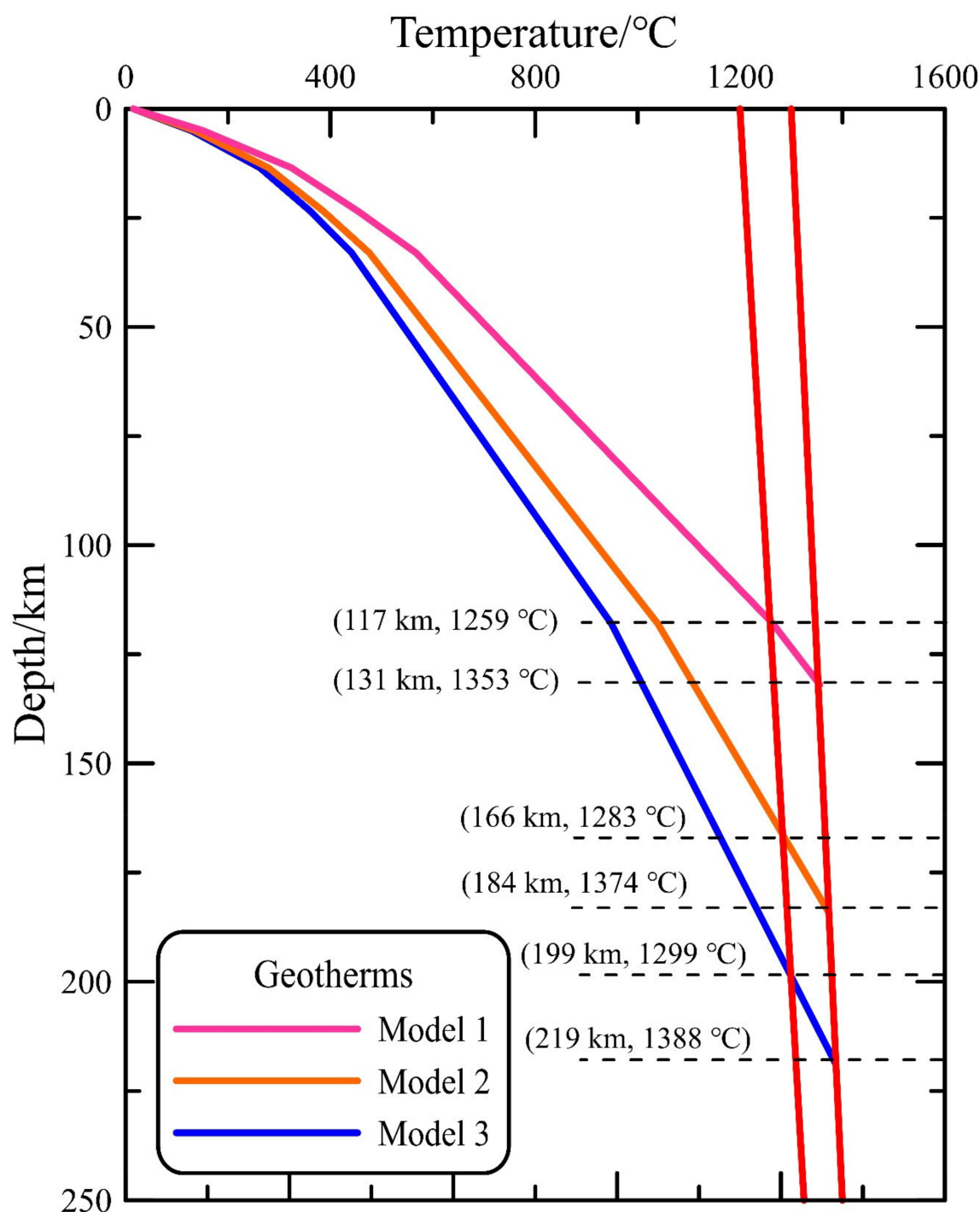


**Figure 6.** Geotherms map of the 3 different models. The red line shows the mantle adiabatic temperature profile.

## 6. Conclusions

By performing thermal conductivity tests in East China, the anisotropic differences in the thermal conductivity of different rock types were studied. The salient conclusions regarding the anisotropic characteristics of thermal conductivity were as follows:

1. The thermal conductivity of different types of rocks varied greatly. Tuff/breccia had the largest fluctuation range of thermal conductivity, 1–11 W/m/K; the largest average value of thermal conductivity was for evaporite, above 5 W/m/K; the smallest was

for unconsolidated rocks, mostly below 2 W/m/K; most rocks did not fluctuate much, mostly between 2 and 5 W/m/K.

2. Thermal conductivity tests were conducted on different rock types parallel and perpendicular to the structural plane, and anisotropic factor of thermal conductivity was calculated. The thermal conductivity anisotropy of unconsolidated rocks and evaporite was not obvious, and basalt/andesite, mudstone, sandstone, carbonate, and regional metamorphic rocks could be regarded as anisotropic. The average anisotropic factor of thermal conductivity of tuff/breccia, granitoid, and contact metamorphic rocks was  $1.19 \pm 0.22$ ,  $1.18 \pm 0.17$ , and  $1.18 \pm 0.17$ , respectively, indicating a strong anisotropic characteristic.
3. Previous thermal conductivity test work performed on surfaces perpendicular to the structural plane probably underestimated the true thermal conductivity values of the rock. Studies on the effect of thermal conductivity anisotropy on heat flow showed that the deviation of the thermal conductivity test may lead to a misperception of deep thermal structure studies.

**Author Contributions:** Conceptualization, Y.W. (Yibo Wang) and G.J.; methodology, Z.W.; software, J.H.; validation, J.H. and S.H.; formal analysis, Y.W. (Yibo Wang) and Y.W. (Yaqi Wang); investigation, Y.W. (Yibo Wang), L.S., Y.R. and Z.W.; data curation, L.S., Y.R. and Z.W.; writing—original draft preparation, Y.W. (Yibo Wang); writing—review and editing, J.H.; visualization, Z.W.; supervision, S.H.; project administration, Y.W. (Yibo Wang); funding acquisition, S.H. All authors have read and agreed to the published version of the manuscript.

**Funding:** This research was accomplished under the support of the State Key Laboratory of Lithospheric Evolution (SKL-K202104), Natural Science Foundation of China (Grant No. 42074096, 42130809), and Shandong Provincial Bureau of Geology & Mineral Resources (202008).

**Data Availability Statement:** The data presented in this study are available on request from the corresponding author. The data are not publicly available due to privacy.

**Acknowledgments:** We are grateful to lecturer Yang Bai of Taiyuan University of Technology, who provided help on the sample collection and treatment that were very important for our research on anisotropic differences in the thermal conductivity of rocks. Best wishes for her first Teacher's Day!

**Conflicts of Interest:** The authors declare no conflict of interest.

## References

1. Rutqvist, J. Thermal management associated with geologic disposal of large spent nuclear fuel canisters in tunnels with thermally engineered backfill. *Tunn. Undergr. Space Technol.* **2020**, *102*, 103454. [\[CrossRef\]](#)
2. Liu, J.; Wang, Z.; Shi, K.; Li, Y.; Liu, L.; Wu, X. Analysis and modeling of thermoelectric power generation in oil wells: A potential power supply for downhole instruments using in-situ geothermal energy. *Renew. Energy* **2020**, *150*, 561–569. [\[CrossRef\]](#)
3. Kharseh, M.; Al-Khawaja, M.; Hassani, F. Optimal utilization of geothermal heat from abandoned oil wells for power generation. *Appl. Therm. Eng.* **2019**, *153*, 536–542. [\[CrossRef\]](#)
4. Zhang, C.; Jiang, G.; Jia, X.; Li, S.; Zhang, S.; Hu, D.; Hu, S.; Wang, Y. Parametric study of the production performance of an enhanced geothermal system: A case study at the Qiabuqia geothermal area, northeast Tibetan plateau. *Renew. Energy* **2019**, *132*, 959–978. [\[CrossRef\]](#)
5. Wang, Z.; Zhang, C.; Jiang, G.; Wang, Y.; Hu, S. Effect of different exploitation schemes on production performance from the carbonate reservoir: A case study in Xiong'an new area. *J. Clean. Prod.* **2021**, *314*, 128050. [\[CrossRef\]](#)
6. Haenel, R.; Rybach, L.; Stegena, L.; Chenb, X. *Handbook of Terrestrial Heat-Flow Density Determination: With Guidelines and Recommendations of the International Heat Flow Commission*; Kluwer Academic Publishers: Dordrecht, The Netherlands, 1988.
7. Davis, M.G.; Chapman, D.S.; Wagoner, T.; Armstrong, P.A. Thermal conductivity anisotropy of metasedimentary and igneous rocks. *J. Geophys. Res. Atmos.* **2007**, *112*, B05216. [\[CrossRef\]](#)
8. Grimmer, J.C.; Jonckheere, R.; Enkelmann, E.; Ratschbacher, L.; Hacker, B.R.; Blythe, A.E.; Wagner, G.A.; Wu, Q.; Liu, S.; Dong, S. Cretaceous—Cenozoic history of the southern Tan-Lu fault zone: Apatite fission-track and structural constraints from the Dabie Shan (Eastern China). *Tectonophysics* **2002**, *359*, 225–253. [\[CrossRef\]](#)
9. Popov, Y.; Beardsmore, G.; Clauser, C.; Roy, S. ISRM Suggested Methods for Determining Thermal Properties of Rocks from Laboratory Tests at Atmospheric Pressure. *Rock Mech. Rock Eng.* **2016**, *49*, 4179–4207. [\[CrossRef\]](#)
10. Popov, Y.A.; Pevzner, S.L.; Pimenov, V.P.; Romushkevich, R.A. New geothermal data from the Kola superdeep well SG-3. *Tectonophysics* **1999**, *306*, 345–366. [\[CrossRef\]](#)

11. He, L.; Hu, S.; Huang, S.; Yang, W.; Wang, J.; Yuan, Y.; Yang, S. Heat flow study at the Chinese Continental Scientific Drilling site: Borehole temperature, thermal conductivity, and radiogenic heat production. *J. Geophys. Res. Solid Earth* **2008**, *113*, B02404. [\[CrossRef\]](#)
12. Wu, S.; Yu, Z.; Kang, J.; Zhang, Y.; Gao, P. Research on the anisotropy of thermal conductivity of rocks in Songliao Basin, China. *Renew. Energy* **2021**, *179*, 593–603. [\[CrossRef\]](#)
13. Birch, F.; Clark, H. The thermal conductivity of rocks and its dependence upon temperature and composition, Part I. *Am. J. Sci.* **1940**, *238*, 529–558. [\[CrossRef\]](#)
14. Barry-Macaulay, D.; Bouazza, A.; Singh, R.M.; Wang, B.; Ranjith, P.G. Thermal conductivity of soils and rocks from the Melbourne (Australia) region. *Eng. Geol.* **2013**, *164*, 131–138. [\[CrossRef\]](#)
15. Meincke, W.; Hurtig, E.; Weiner, J.C. Temperaturerteilung, Wärmeleitfähigkeit und Wärmefluss in Thüringer Becken. *Geophys. Und Geol.* **1967**, *11*, 40–71.
16. Hurtig, E. Untersuchungen der Wärmeleitfähigkeitsanisotropie von Sandsteinen, Grauwacken und Quarziten. *Pure Appl. Geophys.* **1965**, *60*, 85–100. [\[CrossRef\]](#)
17. Birch, F. Flow of heat in the Front Range, Colorado. *Geol. Soc. Am. Bull.* **1950**, *61*, 567–630. [\[CrossRef\]](#)
18. Clark, S.P.; Niblett, E.R. Terrestrial Heat Flow in the Swiss Alps. *Geophys. J. R. Astron. Soc.* **1956**, *7*, 176–195. [\[CrossRef\]](#)
19. Clark, S.P. *Handbook of Physical Constants*; Geological Society of America: Boulder, CO, USA, 1966; Volume 97. [\[CrossRef\]](#)
20. Clark, S.P. Heat Flow in the Austrian Alps. *Geophys. J. R. Astron. Soc.* **1961**, *6*, 54–63. [\[CrossRef\]](#)
21. Sass, J.H.; Marne, A. Heat Flow at Broken Hill, New South Wales. *Geophys. J. R. Astron. Soc.* **1963**, *7*, 477–489. [\[CrossRef\]](#)
22. Diment, W.H.; Werre, R.W. Terrestrial Heat Flow near Washington, D.C. *J. Geophys. Res.* **1964**, *69*, 2143–2149. [\[CrossRef\]](#)
23. Diment, W.H.; Marine, I.W.; Neihsel, J.; Siple, G.E. Subsurface temperature, thermal conductivity, and heat flow near Aiken, South Carolina. *J. Geophys. Res.* **1965**, *70*, 5635–5644. [\[CrossRef\]](#)
24. Robertson, E.C. *Thermal Properties of Rocks*; USGS: Reston, VA, USA, 1988; p. 110.
25. Pribnow, D.; Sass, J.H. Determination of thermal conductivity for deep boreholes. *J. Geophys. Res. Solid Earth* **1995**, *100*, 9981–9994. [\[CrossRef\]](#)
26. Midttomme, K.; Roaldset, E.; Aagaard, K. Thermal Conductivity of Selected Claystones and Mudstones from England. *Clay Min.* **1998**, *33*, 131–145. [\[CrossRef\]](#)
27. Midttomme, K.; Roaldset, E. Thermal conductivity of sedimentary rocks: Uncertainties in measurement and modelling. *Geol. Soc. Lond. Spec. Publ.* **1999**, *158*, 45–60. [\[CrossRef\]](#)
28. Jorand, R.; Vogt, C.; Marquart, G.; Clauser, C. Effective thermal conductivity of heterogeneous rocks from laboratory experiments and numerical modeling. *J. Geophys. Res. Solid Earth* **2013**, *118*, 5225–5235. [\[CrossRef\]](#)
29. Carslaw, H.S.; Jaeger, J.C.; Morral, J.E. Conduction of Heat in Solids, Second Edition. *J. Eng. Mater. Technol.* **1992**, *108*, 378. [\[CrossRef\]](#)
30. Kim, H.; Cho, J.W.; Song, I.; Min, K.B. Anisotropy of elastic moduli, P-wave velocities, and thermal conductivities of Asan Gneiss, Boryeong Shale, and Yeoncheon Schist in Korea. *Eng. Geol.* **2012**, *147–148*, 68–77. [\[CrossRef\]](#)
31. Shi, Y. Lithospheric Thermal Structure and Geothermal Resource of Northern Songliao Basin, NE China. Ph.D. Thesis, University of Chinese Academy of Sciences, Beijing, China, 2019.
32. Mottaghy, D.; Schellschmidt, R.; Popov, Y.A.; Clauser, C.; Kukkonen, I.T.; Nover, G.; Milanovsky, S.; Romushkevich, R.A. New heat flow data from the immediate vicinity of the Kola super-deep borehole: Vertical variation in heat flow confirmed and attributed to advection. *Tectonophysics* **2005**, *401*, 119–142. [\[CrossRef\]](#)
33. Clauser, C.; Giese, P.; Huenges, E.; Kohl, T.; Lehmann, H.; Rybach, L.; Šafanda, J.; Wilhelm, H.; Windloff, K.; Zoth, G. The thermal regime of the crystalline continental crust: Implications from the KTB. *J. Geophys. Res. Solid Earth* **1997**, *102*, 18417–18441. [\[CrossRef\]](#)
34. Wang, Y.; Hu, D.; Wang, L.; Guan, J.; Bai, Y.; Wang, Z.; Jiang, G.; Hu, J.; Tang, B.; Zhu, C.; et al. The present-day geothermal regime of the North Jiangsu Basin, East China. *Geothermics* **2020**, *88*, 101829. [\[CrossRef\]](#)
35. Wang, Y.; Hu, S.; Wang, Z.; Jiang, G.; Hu, D.; Zhang, K.; Gao, P.; Hu, J.; Zhang, T. Heat flow, heat production, thermal structure and its tectonic implication of the southern Tan-Lu Fault Zone, East-Central China. *Geothermics* **2019**, *82*, 254–266. [\[CrossRef\]](#)
36. Wang, Y. Differences of Thermal Regime of the Cratons in Eastern China and Discussion of Its Deep Dynamic Mechanism. Ph.D. Thesis, University of Chinese Academy of Sciences, Beijing, China, 2020.
37. Jiang, G.; Hu, S.; Shi, Y.; Zhang, C.; Wang, Z.; Hu, D. Terrestrial heat flow of continental China: Updated dataset and tectonic implications. *Tectonophysics* **2019**, *753*, 36–48. [\[CrossRef\]](#)
38. Furlong, K.P.; Chapman, D.S. Heat Flow, Heat Generation, and the Thermal State of the Lithosphere. *Annu. Rev. Earth Planet. Sci.* **2013**, *41*, 385–410. [\[CrossRef\]](#)